Analytical and Numerical Solutions for Nonlinear Equations
©Available online at https://ansne.du.ac.ir/
Online ISSN: 3060–785X
2027, Volume 12, Issue 1, pp. 140–161
Research article

Cubic Trigonometric B-Spline VO-L1 Collocation for Variable-Order Caputo Diffusion

Marzieh Khalili[1], Javad Damirchi[1,*], Saedeh Foadian[2]

[1] Department of Mathematics, Faculty of Mathematics, Statistics and Computer Sciences, Semnan University, Semnan, Iran

[2] School of Mathematics and Computer Science, Damghan University, Damghan, Iran

* **Corresponding author(s):** damirchi@semnan.ac.ir

Received: 31/08/2026 **Revised:** 23/09/2026 **Accepted:** 02/10/2026 **Published:** 02/11/2026 10.22128/ansne.2026.3451.1240

Abstract

Variable-order (VO) fractional diffusion equations provide a flexible framework for modeling transport phenomena with time-dependent memory effects. However, the nonlocality of fractional operators, combined with the variable-order structure, makes the development of stable and accurate numerical schemes considerably more challenging. In this paper, a fully discrete numerical method is developed for VO time-fractional diffusion equations involving the Caputo fractional derivative. The spatial discretization is based on cubic trigonometric B-spline collocation, which provides a smooth approximation to the spatial solution. For the temporal discretization, an adapted VO–L1 scheme is employed to approximate the VO Caputo derivative. The variable-order function $\lambda(t)$ incorporates the time-dependent memory effects into the model, and the global temporal convergence rate is of order $2-\lambda_{\max}$, where $\lambda_{\max} = \max_{0\le t\le T_F} \lambda(t)$. By incorporating the Dirichlet boundary conditions into the collocation formulation, the fully discrete system reduces at each time level to a tridiagonal linear algebraic system, which can be solved efficiently. A matrix-based stability analysis is carried out under suitable assumptions on the coefficient matrix. Moreover, a convergence analysis is provided by combining the consistency of the temporal and spatial discretizations with the stability of the overall scheme. Under appropriate regularity assumptions, the proposed method satisfies the global maximum-norm error estimate $\|\mathbf{e}^n\|_\infty \le C\left(h_x^2 + h_t^{2-\lambda_{\max}}\right)$, where C is independent of h_x and h_t. Several numerical experiments are conducted to validate the theoretical findings and assess the accuracy and efficiency of the proposed approach. The results support the theoretical analysis and demonstrate the effectiveness of the cubic trigonometric B-spline VO–L1 collocation scheme for solving VO fractional diffusion problems with time-dependent memory effects.

Keywords: VO timefractional diffusion equation, Caputo VO derivative, Cubic trigonometric Bspline collocation, VO–L1 temporal discretization, Stability, Error analysis.

Mathematics Subject Classification (2020): 65M12, 65M70, 26A33, 35R11

COPYRIGHTS: ©2027, Analytical and Numerical Solutions for Nonlinear Equations published by Damghan University.
This is an open access article published under the *CC BY 4 DEED* license

1 Introduction

Fractional differential equations (FDEs) have become an important mathematical framework for modeling physical and engineering phenomena characterized by memory and hereditary effects. In contrast to classical integer-order models, fractional derivatives incorporate nonlocal temporal behavior and can therefore provide a more flexible description of anomalous diffusion, viscoelasticity, transport processes, and other systems with memory effects [1–4]. Among the various classes of fractional models, time-fractional diffusion equations have received considerable attention because of their ability to describe anomalous transport and diffusion processes with temporal memory. In many applications, however, the memory properties of a physical system may evolve with time. In such cases, the use of a constant fractional order may not adequately represent the underlying dynamics.

VO fractional calculus provides a natural generalization of constant-order fractional models by allowing the order of differentiation to vary with time, space, or both. This additional flexibility has made VO fractional models useful in the mathematical description of heterogeneous and time-dependent processes [5–7]. Nevertheless, the variable fractional order also leads to additional analytical and computational difficulties, particularly because the associated memory kernel changes with time. Therefore, the development of accurate and computationally efficient numerical methods for VO time-fractional partial differential equations remains an important research topic. Various numerical approaches have been developed, including finite difference methods, spectral methods, polynomial approximations, and collocation techniques [8–10]. Among these methods, spline-based collocation schemes are particularly attractive because they provide smooth approximations and lead to structured algebraic systems.

B-spline collocation methods have been successfully applied to several fractional diffusion and diffusion-wave problems [11–14]. In particular, cubic trigonometric B-splines provide a smooth spline basis with trigonometric structure and have been employed in the numerical solution of various fractional and nonlinear differential equations [15–18]. Their local support also leads to sparse algebraic systems, which is advantageous for large-scale computations. Despite the development of several numerical methods for VO fractional models, the combination of cubic trigonometric B-spline collocation with a VO–L1 approximation for the numerical solution of VO time-fractional diffusion equations has received comparatively limited attention. This motivates the development of an efficient fully discrete method that combines the spatial approximation properties of cubic trigonometric B-splines with the nonlocal temporal discretization of the VO Caputo derivative.

In this work, we propose a fully discrete cubic trigonometric B-spline collocation method for the numerical solution of a VO time-fractional diffusion equation. The spatial differential operator is discretized by means of cubic trigonometric B-spline collocation, while the VO Caputo derivative is approximated using a VO–L1 formula. The resulting method leads to a sparse tridiagonal linear algebraic system at each time level. The proposed method can be applied to model anomalous diffusion in heterogeneous materials, biological systems, and other processes where memory effects evolve with time.

The main contributions of this work are summarized as follows:

- A fully discrete numerical method is developed for VO time-fractional diffusion equations by combining cubic trigonometric B-spline collocation in space with a VO–L1 approximation in time.
- The resulting discrete formulation leads to a sparse tridiagonal linear algebraic system at each time level, which can be solved efficiently.
- The consistency, stability, and convergence properties of the proposed numerical scheme are investigated. In particular, the analysis establishes second-order spatial accuracy together with a global temporal error bound governed by the variable fractional order.
- The performance of the proposed method is examined through manufactured-solution experiments using the maximum norm and the root-mean-square error. The numerical results are used to verify the theoretical convergence behavior and assess the accuracy of the proposed scheme.

The remainder of this paper is organized as follows. Section 2 introduces the mathematical model together with the required preliminaries. The cubic trigonometric B-spline spatial discretization is presented in Section 3. The VO–L1 temporal discretization is developed in Section 4. The resulting fully discrete numerical scheme is constructed in Section 5, while its matrix formulation is presented in Section 6. The stability and convergence analyses of the proposed method are presented in Section 7. Numerical experiments are reported in Section 8, and concluding remarks are given in Section 9.

2 Preliminaries and Mathematical Model

In this section, we introduce the VO time-fractional diffusion model considered throughout this work and present the mathematical preliminaries required for the development and analysis of the proposed numerical method.

Let $\overline{\Omega} = (0,1)$ and $0 < t \le T_F$, and consider the VO time-fractional diffusion equation

$$ {}_0^C\mathscr{D}_t^{\lambda(t)}\Phi(x,t) = \rho\frac{\partial^2\Phi(x,t)}{\partial x^2} + \mathscr{F}(x,t), \qquad (x,t) \in \overline{\Omega}\times(0,T_F], \tag{1}$$

where ${}_0^C\mathscr{D}_t^{\lambda(t)}$ denotes the VO Caputo fractional derivative, $\rho > 0$ is the diffusion coefficient, and $\mathscr{F}(x,t)$ is a prescribed source function.

The problem is supplemented with the initial condition

$$\Phi(x,0) = \varphi(x), \qquad x \in \overline{\Omega},$$

and the Dirichlet boundary conditions

$$\Phi(0,t) = g_1(t), \qquad \Phi(1,t) = g_2(t), \qquad 0 < t \le T_F.$$

The variable fractional order is assumed to satisfy

$$0 < \lambda_{\min} \le \lambda(t) \le \lambda_{\max} < 1, \qquad \lambda(t) \in C^1([0,T_F]),$$

where $\lambda_{\min}$ and $\lambda_{\max}$ are positive constants. This assumption guarantees that the fractional order varies continuously in time while remaining inside the admissible interval $(0,1)$.

For the consistency and convergence analysis, the exact solution is assumed to satisfy $\Phi \in C^{4,2}\left(\overline{\Omega}\times[0,T_F]\right)$ while the functions $\varphi(x)$, $g_1(t)$, $g_2(t)$, and $\mathscr{F}(x,t)$ are assumed to be sufficiently smooth and mutually compatible.

The model problem (1) extends the classical constant-order time-fractional diffusion equation by allowing the fractional order to vary with time. Consequently, the associated memory effects evolve throughout the diffusion process, providing additional flexibility for modeling anomalous transport and diffusion phenomena with time-dependent hereditary behavior.

For the numerical approximation, the spatial domain $\overline{\Omega} = [0,1]$ is discretized by a uniform spatial grid, while the temporal interval $[0,T_F]$ is discretized by a uniform time grid. The precise definitions of the spatial and temporal mesh points, together with the corresponding mesh sizes, are introduced in the subsequent spatial and temporal discretization sections.

The VO Caputo fractional derivative is defined by

$$ {}_0^C\mathscr{D}_t^{\lambda(t)}\Phi(x,t) = \frac{1}{\Gamma(1-\lambda(t))}\int_0^t \frac{\partial\Phi(x,s)/\partial s}{(t-s)^{\lambda(t)}}\,ds, \qquad 0 < \lambda(t) < 1. \tag{2}$$

Unlike the classical Caputo operator, the fractional order varies continuously with time. Consequently, the memory kernel changes throughout the diffusion process, allowing the model to describe anomalous diffusion with time-dependent hereditary effects. This additional flexibility makes VO fractional models particularly suitable for applications in which the memory characteristics evolve over time [5–7].

The operator (2) is nonlocal in time since its value at any given time depends on the entire history of the solution over the interval $[0,t]$. As in the classical Caputo formulation, the VO Caputo derivative of a constant is identically zero, ${}_0^C\mathscr{D}_t^{\lambda(t)}C = 0$. This property ensures the consistent treatment of the initial condition in the fractional diffusion model.

Throughout this work, the VO Caputo derivative is approximated by the variable-order L1 (VO–L1) finite-difference formula, while the spatial differential operator is discretized using cubic trigonometric B-spline collocation. The resulting fully discrete numerical formulation is developed in the following sections.

3 Spatial Discretization Via Cubic Trigonometric B-Splines

In this section, the spatial differential operator in the VO time-fractional diffusion equation is discretized using cubic trigonometric B-spline collocation. The compact support and smoothness of the cubic trigonometric B-spline basis lead to a structured and sparse spatial discretization, which is well suited for the numerical approximation of the diffusion operator.

Let the computational domain $\overline{\Omega} = [0,1]$ be divided into M uniform spatial subintervals according to $0 = x_0 < x_1 < \cdots < x_M = 1$, where $x_i = ih_x$, $i = 0,1,\ldots,M$, and $h_x = \frac{1}{M}$. To construct the cubic trigonometric B-spline basis near the boundary of the physical domain, two auxiliary knots are introduced outside the computational interval x_{-1}, and x_{M+1}. Thus, the extended grid is given by $x_{-1} < x_0 < x_1 < \cdots < x_M < x_{M+1}$. The auxiliary knots are introduced solely for the construction of the spline basis and do not represent additional physical grid points. The corresponding auxiliary spline coefficients are subsequently eliminated or incorporated through the prescribed boundary conditions.

Let $\{T_i(x)\}_{i=-1}^{M+1}$ denote the cubic trigonometric B-spline basis functions associated with the extended grid. Each basis function has compact support over a finite number of neighboring subintervals. Consequently, only a small number of basis functions contribute at any given collocation point.

At the time level t_n, the continuous spline approximation to the numerical solution is represented by

$$U_N(x,t_n) = \sum_{i=-1}^{M+1} C_i^n T_i(x), \tag{3}$$

where C_i^n are the unknown spline coefficients at the time level t_n.

The compact support of the basis functions implies that the value of the spline approximation and its spatial derivatives at a grid point depend only on neighboring spline coefficients. This local structure is the main reason for the sparse algebraic systems obtained from the collocation procedure.

In the following subsection, the nodal values of the cubic trigonometric B-spline approximation and its first- and second-order spatial derivatives are evaluated explicitly at the collocation points. These relations are then used to construct the fully discrete numerical scheme.

3.1 Cubic Trigonometric B-Spline Basis Functions

Let $\{T_i(x)\}_{i=-1}^{M+1}$ denote the family of cubic trigonometric B-spline basis functions associated with the extended uniform grid. These basis functions are locally supported, nonnegative, and sufficiently smooth for the collocation of the second-order spatial differential operator. In particular, $T_i(x) \geq 0$ and, on the computational interval $\overline{\Omega} = [0,1]$, they satisfy the partition of unity property $\sum_{i=-1}^{M+1} T_i(x) = 1$. Moreover, $T_i(x) \in C^2(\overline{\Omega})$, which ensures the continuity of the basis functions and their first and second derivatives across the interior grid points.

The support of each basis function is local and is given by $\mathrm{supp}(T_i) = [x_{i-2}, x_{i+2}]$. Consequently, only a limited number of neighboring basis functions contribute to the numerical approximation at any collocation point. This local support leads to the sparse structure of the algebraic system resulting from the collocation procedure.

For the construction of the cubic trigonometric B-spline basis, define

$$\omega_i(x) = \sin\left(\frac{x - x_i}{2}\right),$$

and introduce the normalization factor

$$\theta = \sin\left(\frac{h_x}{2}\right)\sin(h_x)\sin\left(\frac{3h_x}{2}\right).$$

The cubic trigonometric B-spline basis function $T_i(x)$ is defined by

$$T_i(x) = \frac{1}{\theta}\begin{cases} \omega_{i-2}^3(x), & x \in [x_{i-2}, x_{i-1}), \\ \omega_{i-2}(x)\Big[\omega_{i-2}(x)\omega_i(x) + \omega_{i-1}(x)\omega_{i+1}(x)\Big] + \omega_{i+1}^2(x)\omega_{i-1}(x), & x \in [x_{i-1}, x_i), \\ \omega_{i-2}(x)\omega_{i+2}^2(x) + \omega_i(x)\Big[\omega_{i-1}(x)\omega_{i+1}(x) + \omega_i(x)\omega_{i+2}(x)\Big], & x \in [x_i, x_{i+1}), \\ \omega_{i+2}^3(x), & x \in [x_{i+1}, x_{i+2}), \\ 0, & \text{otherwise}. \end{cases} \tag{4}$$

The normalization in (4), together with the uniform grid structure, yields a C^2-continuous cubic trigonometric B-spline basis. In particular, the basis functions and their first and second derivatives are continuous across the interior knots. Therefore, the basis is suitable for the collocation of the second-order diffusion operator appearing in (1).

3.2 Spline Approximation and Nodal Relations

Using the cubic trigonometric B-spline approximation (3), the approximate solution and its spatial derivatives are evaluated at the collocation points $x = x_i$, $i = 0, 1, \ldots, M$. This yields the following local nodal relations:

$$U_N(x_i,t_n) = A_1C_{i-1}^n + A_2C_i^n + A_1C_{i+1}^n, \qquad U_N(x_i,t_n) \approx \Phi(x_i,t_n), \tag{5}$$

$$\frac{\partial U_N}{\partial x}(x_i,t_n) = A_3C_{i-1}^n + A_4C_{i+1}^n, \qquad \frac{\partial U_N}{\partial x}(x_i,t_n) \approx \frac{\partial \Phi}{\partial x}(x_i,t_n), \tag{6}$$

$$\frac{\partial^2 U_N}{\partial x^2}(x_i,t_n) = A_5C_{i-1}^n + A_6C_i^n + A_5C_{i+1}^n, \qquad \frac{\partial^2 U_N}{\partial x^2}(x_i,t_n) \approx \frac{\partial^2 \Phi}{\partial x^2}(x_i,t_n). \tag{7}$$

The coefficients appearing in the above nodal relations depend only on the spatial mesh size h_x and are given by

$$A_1 = \frac{\sin^2(h_x/2)}{\sin(h_x)\sin(3h_x/2)}, \qquad A_2 = \frac{2}{1+2\cos(h_x)}, \qquad A_3 = -\frac{3}{4\sin(3h_x/2)},$$

$$A_4 = \frac{3}{4\sin(3h_x/2)}, \qquad A_5 = \frac{3(1+3\cos h_x)}{16\sin^2(h_x/2)\,(2\cos(h_x/2)+\cos(3h_x/2))}, \qquad A_6 = -\frac{3\cos^2(h_x/2)}{\sin^2(h_x/2)(2+4\cos h_x)}.$$

Equations (5)–(7) establish the relationship between the spline coefficients $\{C_i^n\}$ and the nodal values of the approximate solution and its spatial derivatives. In particular, (7) is employed to discretize the diffusion term in (1), whereas (5) provides the approximation of the solution at the collocation points. These nodal relations constitute the foundation of the cubic trigonometric B-spline collocation discretization developed in the following subsections.

3.3 Boundary Elimination

Because the cubic trigonometric B-spline approximation involves the auxiliary spline coefficients C_{-1}^n and C_{M+1}^n, these coefficients must be eliminated from the discrete system. Applying the nodal relation (5) at the boundary collocation points gives

$$U_N(0,t_n) = A_1C_{-1}^n + A_2C_0^n + A_1C_1^n,$$

and

$$U_N(1,t_n) = A_1C_{M-1}^n + A_2C_M^n + A_1C_{M+1}^n.$$

Applying the prescribed Dirichlet boundary conditions introduced in Section 2, the auxiliary spline coefficients can be written as

$$C_{-1}^n = \frac{g_1(t_n) - A_2C_0^n - A_1C_1^n}{A_1}, \tag{8}$$

and

$$C_{M+1}^n = \frac{g_2(t_n) - A_1C_{M-1}^n - A_2C_M^n}{A_1}. \tag{9}$$

Substituting (8) and (9) into the fully discrete collocation equations eliminates the two auxiliary spline coefficients C_{-1}^n and C_{M+1}^n. However, the boundary spline coefficients C_0^n and C_M^n remain unknown and are retained as physical spline coefficients. The resulting algebraic system is therefore formulated in terms of the physical spline coefficient vector $\mathbf{C}^n = \left[C_0^n, C_1^n, \ldots, C_M^n\right]^T$.

3.4 Initialization of Spline Coefficients

At the initial time level $t_0 = 0$, the spline coefficients are determined from the prescribed initial condition together with the cubic trigonometric B-spline nodal relations. Let

$$C_i^0 := C_i(t_0), \qquad i = -1, 0, \ldots, M+1,$$

denote the spline coefficients at the initial time level.

The initial condition is imposed at the spatial collocation points x_i, $i = 0, 1, \ldots, M$, through

$$A_1C_{i-1}^0 + A_2C_i^0 + A_1C_{i+1}^0 = \varphi(x_i), \qquad i = 0, 1, \ldots, M. \tag{10}$$

At the two boundary points, the derivative of the initial condition is also incorporated through the corresponding first-derivative nodal relation. Thus,

$$\frac{\partial U_N}{\partial x}(x_i,t_0)=\varphi'(x_i),\qquad i=0,M.$$

At the left boundary point $x=x_0$, using (6) gives $A_3C^0_{-1}+A_4C^0_1=\varphi'(x_0)$. Therefore,

$$C^0_{-1}=\frac{\varphi'(x_0)-A_4C^0_1}{A_3}.$$

Substituting this expression into the initial-condition relation (10) at $i=0$ eliminates the auxiliary coefficient C^0_{-1} and gives

$$A_2C^0_0+\left(A_1-\frac{A_1A_4}{A_3}\right)C^0_1=\varphi(x_0)-\frac{A_1}{A_3}\varphi'(x_0). \tag{11}$$

Similarly, at the right boundary point $x=x_M$, the first-derivative nodal relation gives $A_3C^0_{M-1}+A_4C^0_{M+1}=\varphi'(x_M)$ and hence

$$C^0_{M+1}=\frac{\varphi'(x_M)-A_3C^0_{M-1}}{A_4}.$$

Substituting this expression into the initial-condition relation (10) at $i=M$ eliminates the auxiliary coefficient C^0_{M+1} and yields

$$\left(A_1-\frac{A_1A_3}{A_4}\right)C^0_{M-1}+A_2C^0_M=\varphi(x_M)-\frac{A_1}{A_4}\varphi'(x_M). \tag{12}$$

Consequently, the two auxiliary coefficients C^0_{-1} and C^0_{M+1} are eliminated from the initialization system. The two boundary relations (11) and (12), together with the interior relations (10) for $i=1,2,\ldots,M-1$, form a closed system for the physical spline coefficients

$$\mathbf{C}^0=\left[C^0_0,C^0_1,\ldots,C^0_M\right]^T.$$

Thus, the initialization problem can be written in matrix form as

$$\mathbf{A}_0\mathbf{C}^0=\mathbf{b}_0, \tag{13}$$

where $\mathbf{A}_0$ is the coefficient matrix generated by the two boundary relations (11)–(12) and the interior relations (10), while $\mathbf{b}_0$ contains the prescribed initial and boundary data.

Because of the local support of the cubic trigonometric B-spline basis, the matrix $\mathbf{A}_0$ is sparse and banded. Consequently, the initial spline coefficients can be computed efficiently by solving (13). Once $\mathbf{C}^0$ is obtained, the auxiliary coefficients C^0_{-1} and C^0_{M+1} are recovered from the first-derivative nodal relations at $x=x_0$ and $x=x_M$, respectively.

4 VO Time Discretization

This section develops the variable-order L1 (VO–L1) approximation for the temporal discretization of the VO Caputo fractional derivative. The derivation is based on a piecewise linear interpolation of the solution over each temporal subinterval. Since the fractional order is evaluated at the current time level, the resulting convolution coefficients become time dependent while preserving the nonlocal memory structure of the VO fractional operator.

4.1 Derivation of the VO--L1 Approximation

At the discrete time levels introduced in Section 2, let

$$\lambda_n=\lambda(t_n),\qquad 0<\lambda_n<1,\qquad n=0,1,\ldots,N.$$

For a fixed time level t_{n+1}, the variable-order Caputo fractional derivative is defined by

$${}^{C}D_t^{\lambda_{n+1}}\Phi(x,t_{n+1})=\frac{1}{\Gamma(1-\lambda_{n+1})}\int_0^{t_{n+1}}(t_{n+1}-\tau)^{-\lambda_{n+1}}\frac{\partial\Phi(x,\tau)}{\partial\tau}\,d\tau. \tag{14}$$

Because the VO Caputo derivative is nonlocal in time, its evaluation at t_{n+1} depends on the entire solution history over $[0,t_{n+1}]$. To construct the L1 approximation, the integral is decomposed over the temporal subintervals $[t_k,t_{k+1}]$, $k=0,1,\ldots,n$, according to

$$\int_0^{t_{n+1}} (t_{n+1}-\tau)^{-\lambda_{n+1}} \frac{\partial \Phi(x,\tau)}{\partial \tau}\, d\tau = \sum_{k=0}^{n} \int_{t_k}^{t_{k+1}} (t_{n+1}-\tau)^{-\lambda_{n+1}} \frac{\partial \Phi(x,\tau)}{\partial \tau}\, d\tau. \tag{15}$$

On each subinterval $[t_k,t_{k+1}]$, the time derivative is approximated by the backward difference

$$\frac{\partial \Phi(x,\tau)}{\partial \tau} \approx \frac{\Phi^{k+1}(x)-\Phi^{k}(x)}{h_t}, \qquad \tau \in [t_k,t_{k+1}], \tag{16}$$

where $\Phi^k(x) := \Phi(x,t_k)$. The kernel integral over each temporal subinterval is

$$\int_{t_k}^{t_{k+1}} (t_{n+1}-\tau)^{-\lambda_{n+1}}\, d\tau = \frac{h_t^{1-\lambda_{n+1}}}{1-\lambda_{n+1}} \left[(n-k+1)^{1-\lambda_{n+1}} - (n-k)^{1-\lambda_{n+1}}\right], \qquad k=0,1,\ldots,n.$$

Using the relation

$$\Gamma(2-\lambda_{n+1}) = (1-\lambda_{n+1})\Gamma(1-\lambda_{n+1}),$$

we introduce the scaling factor

$$\gamma_{n+1} = \frac{h_t^{-\lambda_{n+1}}}{\Gamma(2-\lambda_{n+1})}.$$

Substitution of the backward difference approximation and the kernel integral into (15) yields the VO–L1 approximation

$${}^{C}D_t^{\lambda_{n+1}} \Phi(x,t_{n+1}) = \gamma_{n+1} \sum_{k=0}^{n} \left[(k+1)^{1-\lambda_{n+1}} - k^{1-\lambda_{n+1}}\right] \left[\Phi^{n+1-k}(x) - \Phi^{n-k}(x)\right] + \mathscr{R}_{n+1}(x), \tag{17}$$

where $\mathscr{R}_{n+1}(x)$ denotes the local truncation error.

Separating the term corresponding to $k=0$ from the remaining history terms gives

$${}^{C}D_t^{\lambda_{n+1}} \Phi(x,t_{n+1}) = \gamma_{n+1} \left[\Phi^{n+1}(x) - \Phi^{n}(x)\right] + \gamma_{n+1} \sum_{k=1}^{n} a_k^{n+1} \left[\Phi^{n+1-k}(x) - \Phi^{n-k}(x)\right] + \mathscr{R}_{n+1}(x), \tag{18}$$

where the VO–L1 memory weights are defined by

$$a_k^{n+1} = (k+1)^{1-\lambda_{n+1}} - k^{1-\lambda_{n+1}}, \qquad k=1,2,\ldots,n.$$

4.2 Properties of the VO--L1 Approximation

The VO–L1 discretization introduced in Section 4 preserves the nonlocal memory structure of the VO Caputo fractional derivative through the time-dependent coefficients a_k^{n+1} appearing in (17)–(18).

For each time level t_{n+1}, the coefficients a_k^{n+1} depend on the local fractional order λ_{n+1} and satisfy

$$a_k^{n+1} > 0, \qquad a_{k+1}^{n+1} < a_k^{n+1}, \qquad k=0,1,\ldots,n-1.$$

Indeed, the function $s^{1-\lambda_{n+1}}$ is increasing and concave for $0<\lambda_{n+1}<1$. Consequently, its successive increments are positive and monotonically decreasing. This monotonicity reflects the gradual decay of the discrete memory contribution and plays an essential role in the stability and convergence analysis of the proposed numerical scheme.

The local truncation error of the VO–L1 approximation satisfies

$$\mathscr{R}_{n+1}(x) = \mathscr{O}\left(h_t^{2-\lambda_{n+1}}\right).$$

Since $\lambda(t) \le \lambda_{\max}$, $0 \le t \le T_F$, the corresponding global temporal accuracy is bounded by $\mathscr{O}(h_t^{2-\lambda_{\max}})$. which is the convergence order established later in Section 7.

The VO–L1 temporal discretization is subsequently combined with the cubic trigonometric B-spline spatial approximation developed in Section 3 to construct the fully discrete numerical scheme presented in the next subsection.

5 Fully Discrete Numerical Scheme

This section combines the cubic trigonometric B-spline collocation discretization developed in Section 3 with the VO–L1 temporal approximation introduced in Section 4 to derive the fully discrete numerical scheme for the variable-order time-fractional diffusion equation.

The spatial approximation represents the numerical solution and its second-order spatial derivative in terms of the cubic trigonometric B-spline coefficients, whereas the time-fractional derivative is approximated by the VO–L1 formula. Combining these two discretizations yields the fully discrete collocation formulation at each time level.

The resulting formulation is first expressed at the collocation points in terms of the spline coefficients at the current and previous time levels. The temporal memory contribution arising from the variable-order fractional derivative is retained explicitly, providing the coefficient-level algebraic form of the fully discrete scheme.

5.1 Fully Discrete Cubic Trigonometric B-Spline VO--L1 Scheme

Substituting the VO–L1 approximation (18) into the governing equation (1), and approximating the spatial derivatives by the cubic trigonometric B-spline collocation relations (5)–(7), yields the fully discrete collocation formulation.

Accordingly, for each interior collocation point x_i, $i = 1,2,\ldots,M-1$, and each time level t_{n+1}, $n \geq 0$, the fully discrete equation is given by

$$\gamma_{n+1}\left[U_N(x_i,t_{n+1}) - U_N(x_i,t_n) + \sum_{k=1}^{n} a_k^{n+1}\left(U_N(x_i,t_{n-k+1}) - U_N(x_i,t_{n-k})\right)\right] = \rho\,\frac{\partial^2 U_N}{\partial x^2}(x_i,t_{n+1}) + \mathscr{F}_i^{n+1}, \tag{19}$$

where $\mathscr{F}_i^{n+1} = \mathscr{F}(x_i,t_{n+1})$. The quantities γ_{n+1} and a_k^{n+1} are determined by the VO–L1 approximation introduced in Section 4.

Using the nodal relations (5) and (7), equation (19) can be written entirely in terms of the spline coefficients as

$$\begin{aligned}\gamma_{n+1}\left[A_1C_{i-1}^{n+1} + A_2C_i^{n+1} + A_1C_{i+1}^{n+1}\right] - \rho\left[A_5C_{i-1}^{n+1} + A_6C_i^{n+1} + A_5C_{i+1}^{n+1}\right] &= \mathscr{F}_i^{n+1} + \gamma_{n+1}\left[A_1C_{i-1}^{n} + A_2C_i^{n} + A_1C_{i+1}^{n}\right] \\ &\quad - \gamma_{n+1}\sum_{k=1}^{n} a_k^{n+1}\left[A_1\left(C_{i-1}^{n-k+1} - C_{i-1}^{n-k}\right) + A_2\left(C_i^{n-k+1} - C_i^{n-k}\right)\right. \\ &\quad \left. + A_1\left(C_{i+1}^{n-k+1} - C_{i+1}^{n-k}\right)\right], \qquad i = 1,2,\ldots,M-1.\end{aligned}$$

To simplify the notation, we introduce the temporal memory contribution at the coefficient level by

$$\mathscr{H}_i^{n+1} = \sum_{k=1}^{n} a_k^{n+1}\left[A_1\left(C_{i-1}^{n-k+1} - C_{i-1}^{n-k}\right) + A_2\left(C_i^{n-k+1} - C_i^{n-k}\right) + A_1\left(C_{i+1}^{n-k+1} - C_{i+1}^{n-k}\right)\right], \tag{20}$$

where the empty sum for $n = 0$ is understood to be zero.

The quantity $\mathscr{H}_i^{n+1}$ represents the accumulated temporal memory contribution generated by the nonlocal variable-order Caputo fractional derivative. It contains the contributions from all previously computed time levels and therefore carries the temporal history of the numerical solution into the current time level.

Using (20), the fully discrete collocation equations can be written in the compact coefficient-level form

$$(\gamma_{n+1}A_1 - \rho A_5)C_{i-1}^{n+1} + (\gamma_{n+1}A_2 - \rho A_6)C_i^{n+1} + (\gamma_{n+1}A_1 - \rho A_5)C_{i+1}^{n+1} = \mathscr{R}_i^{n+1}, \tag{21}$$

where

$$\mathscr{R}_i^{n+1} = \mathscr{F}_i^{n+1} + \gamma_{n+1}\left(A_1C_{i-1}^{n} + A_2C_i^{n} + A_1C_{i+1}^{n}\right) - \gamma_{n+1}\mathscr{H}_i^{n+1}. \tag{22}$$

Equations (21)–(22) constitute the fully discrete cubic trigonometric B-spline VO–L1 collocation scheme at the interior collocation points. The coefficient-level formulation separates the contribution from the current time level from the previously computed solution, the source term, and the accumulated temporal memory.

For $n = 0$, the memory contribution $\mathscr{H}_i^{1}$ is zero because the summation in (20) is empty. Thus, the first time step involves only the current and initial solution contributions together with the source term.

The coefficient-level equations (21)–(22) provide the starting point for the algebraic system at each time level. The corresponding tridiagonal structure and the incorporation of the prescribed Dirichlet boundary conditions are discussed in the next subsection.

6 Matrix Formulation of the Numerical Scheme

In this section, the fully discrete cubic trigonometric B-spline collocation scheme derived in Section 5 is reformulated in matrix form. This representation provides a compact description of the resulting algebraic system and makes its sparse and tridiagonal structure explicit. In particular, the time-dependent coefficients of the system reflect the dependence of the VO–L1 discretization on the fractional order at the current time level.

The matrix formulation also provides a convenient framework for the successive solution of the algebraic system at each time level and serves as the basis for the solvability, stability, and convergence analyses presented in the subsequent sections.

6.1 Algebraic System at Each Time Level

For each time level t_{n+1}, $n \geq 0$, the fully discrete collocation equations derived in Section 5 are considered at the interior collocation points x_i, $i = 1,2,\ldots,M-1$. Using the nodal relations (5) and (7), the fully discrete formulation (21) can be expressed in terms of the spline coefficients as

$$(\gamma_{n+1}A_1 - \rho A_5)C_{i-1}^{n+1} + (\gamma_{n+1}A_2 - \rho A_6)C_i^{n+1} + (\gamma_{n+1}A_1 - \rho A_5)C_{i+1}^{n+1} = \mathscr{R}_i^{n+1}, \qquad i = 1,2,\ldots,M-1, \tag{23}$$

where γ_{n+1} and the memory weights a_k^{n+1} are determined by the local fractional order $\lambda_{n+1} = \lambda(t_{n+1})$. The right-hand side $\mathscr{R}_i^{n+1}$ is the quantity defined in (22) and contains the source contribution, the contribution from the previous time level, and the accumulated temporal memory contribution $\mathscr{H}_i^{n+1}$.

The history contribution $\mathscr{H}_i^{n+1}$, defined in (20), contains only previously computed time levels. Therefore, at the first time step, $n = 0$, the summation in (20) is empty and is taken to be zero. Consequently, no contribution from earlier time levels is present in the history term at the first time level.

For convenience, we introduce the time-level-dependent coefficients

$$\theta_1^{n+1} = \gamma_{n+1}A_1 - \rho A_5, \qquad \theta_2^{n+1} = \gamma_{n+1}A_2 - \rho A_6.$$

Then (23) takes the compact form

$$\theta_1^{n+1}C_{i-1}^{n+1} + \theta_2^{n+1}C_i^{n+1} + \theta_1^{n+1}C_{i+1}^{n+1} = \mathscr{R}_i^{n+1}, \qquad i = 1,2,\ldots,M-1. \tag{24}$$

Thus, the interior collocation equations possess a tridiagonal coefficient stencil, with identical off-diagonal coefficients. Moreover, the corresponding interior stencil is symmetric. Since γ_{n+1} depends on the local fractional order λ_{n+1}, the coefficients θ_1^{n+1} and θ_2^{n+1} may change from one time level to another. Hence, the coefficient matrix is, in general, updated at each time level.

The equations in (24) still involve the auxiliary spline coefficients C_{-1}^{n+1} and C_{M+1}^{n+1} near the two boundaries. These coefficients do not represent additional physical grid points; rather, they are auxiliary coefficients introduced for the construction of the cubic trigonometric B-spline basis. They are eliminated by means of the boundary relations derived in Section 3.

For each time level t_{n+1}, the complete collocation formulation is initially associated with the $M+1$ physical collocation points $i = 0,1,\ldots,M$ and the $M+3$ spline coefficients $C_{-1}^{n+1}, C_0^{n+1}, \ldots, C_M^{n+1}, C_{M+1}^{n+1}$. The prescribed Dirichlet boundary conditions are first used to eliminate the two auxiliary spline coefficients C_{-1}^{n+1} and C_{M+1}^{n+1}. The resulting boundary relations are then substituted into the collocation equations at the two boundary points $i = 0$ and $i = M$. In this way, the boundary equations are retained as algebraic equations for the physical spline coefficients.

Consequently, after elimination of the two auxiliary coefficients, the remaining unknown vector is $\mathbf{C}^{n+1} = \left[C_0^{n+1}, C_1^{n+1}, \ldots, C_M^{n+1}\right]^T$, which contains $M+1$ unknown physical spline coefficients. The $M-1$ interior collocation equations together with the two boundary-corrected collocation equations provide exactly $M+1$ equations. Hence, the final algebraic system is a square system of dimension $M+1$.

6.2 Matrix Representation and Boundary Incorporation

Using the compact algebraic relation (24), the interior collocation equations at the time level t_{n+1} can be assembled into a tridiagonal linear system. Before incorporating the boundary conditions, the interior equations have the matrix representation

$$\mathbf{K}_{\text{int}}^{n+1}\mathbf{C}_{\text{int}}^{n+1} = \mathbf{R}_{\text{int}}^{n+1}, \tag{25}$$

where

$$\mathbf{C}_{\text{int}}^{n+1} = \left[C_1^{n+1}, C_2^{n+1}, \ldots, C_{M-1}^{n+1}\right]^T \tag{26}$$

denotes the vector of interior spline coefficients. The corresponding coefficient matrix is tridiagonal and is given by

$$\mathbf{K}_{\text{int}}^{n+1} = \begin{bmatrix} \theta_2^{n+1} & \theta_1^{n+1} & 0 & \cdots & 0 \\ \theta_1^{n+1} & \theta_2^{n+1} & \theta_1^{n+1} & \ddots & \vdots \\ 0 & \theta_1^{n+1} & \theta_2^{n+1} & \ddots & 0 \\ \vdots & \ddots & \ddots & \ddots & \theta_1^{n+1} \\ 0 & \cdots & 0 & \theta_1^{n+1} & \theta_2^{n+1} \end{bmatrix}. \tag{27}$$

The tridiagonal structure follows from the local support of the cubic trigonometric B-spline basis. The coefficients θ_1^{n+1} and θ_2^{n+1} depend on the current fractional order through γ_{n+1} and $\lambda_{n+1} = \lambda(t_{n+1})$. Therefore, the coefficient matrix may change from one time level to another. The interior matrix is symmetric because its two off-diagonal coefficients are identical.

The auxiliary spline coefficients C_{-1}^{n+1} and C_{M+1}^{n+1} are eliminated using the boundary relations (8) and (9), respectively. Substituting these relations into the collocation equations at the two boundary points eliminates the auxiliary coefficients from the algebraic system.

At the left boundary, the collocation equation contains C_{-1}^{n+1}, C_0^{n+1}, and C_1^{n+1}. Substitution of (8) causes the coefficient of C_1^{n+1} to cancel. Consequently, the first row of the final algebraic system contains only the coefficient associated with C_0^{n+1}. Similarly, at the right boundary, substitution of (9) causes the coefficient of C_{M-1}^{n+1} to cancel, and therefore the last row contains only the coefficient associated with C_M^{n+1}.

After elimination of the two auxiliary coefficients, the remaining unknowns are the physical spline coefficients

$$\mathbf{C}^{n+1} = \left[C_0^{n+1}, C_1^{n+1}, \ldots, C_M^{n+1}\right]^T. \tag{28}$$

The $M-1$ interior collocation equations together with the two boundary-corrected equations therefore provide exactly $M+1$ equations for the $M+1$ physical spline coefficients.

Accordingly, the complete algebraic system at the time level t_{n+1} can be written as

$$\mathbf{K}^{n+1}\mathbf{C}^{n+1} = \mathbf{R}^{n+1}, \tag{29}$$

where the coefficient matrix is

$$\mathbf{K}^{n+1} = \begin{bmatrix} \theta_2^{n+1} - \dfrac{A_2}{A_1}\theta_1^{n+1} & 0 & 0 & \cdots & 0 \\ \theta_1^{n+1} & \theta_2^{n+1} & \theta_1^{n+1} & \ddots & \vdots \\ 0 & \theta_1^{n+1} & \theta_2^{n+1} & \ddots & 0 \\ \vdots & \ddots & \ddots & \ddots & \theta_1^{n+1} \\ 0 & \cdots & 0 & 0 & \theta_2^{n+1} - \dfrac{A_2}{A_1}\theta_1^{n+1} \end{bmatrix}. \tag{30}$$

Thus, the first and last diagonal entries are modified by the elimination of the auxiliary spline coefficients, while the interior diagonal and off-diagonal entries remain unchanged. In particular, the boundary elimination also removes the first off-diagonal entry in the first row and the last off-diagonal entry in the last row. Hence, the resulting matrix remains tridiagonal, but in general it is not symmetric.

The corresponding right-hand-side vector is written as

$$\mathbf{R}^{n+1} = \left[\mathscr{R}_0^{n+1} - \frac{\theta_1^{n+1}}{A_1} g_1(t_{n+1}), \mathscr{R}_1^{n+1}, \ldots, \mathscr{R}_{M-1}^{n+1}, \mathscr{R}_M^{n+1} - \frac{\theta_1^{n+1}}{A_1} g_2(t_{n+1})\right]^T, \tag{31}$$

where $\mathscr{R}_0^{n+1}$ and $\mathscr{R}_M^{n+1}$ denote the right-hand-side expressions associated with the collocation equations at the two boundary points before elimination of the auxiliary spline coefficients, while $\mathscr{R}_i^{n+1}$, $i = 1, \ldots, M-1$, are given by (22).

Therefore, the boundary-elimination procedure preserves the sparse tridiagonal structure of the algebraic system, while modifying the first and last rows according to the prescribed Dirichlet boundary conditions. The resulting system can be solved at each time level by a standard tridiagonal linear-system solver, such as the Thomas algorithm, provided the coefficient matrix is nonsingular.

The matrix formulation obtained above provides the algebraic framework required for the subsequent stability and convergence analysis of the proposed numerical method.

6.3 Solution of the Linear System

At each time level t_{n+1}, the fully discrete numerical scheme leads to the linear algebraic system (29), where the coefficient matrix $\mathbf{K}^{n+1}$ is sparse and tridiagonal, while the right-hand-side vector contains the source term, the contribution from the previous time level, the accumulated temporal memory contribution, and the prescribed boundary data.

Since the coefficient matrix is tridiagonal, the resulting linear system can be solved efficiently using the Thomas algorithm, which is a direct solver specifically designed for tridiagonal systems. The solution procedure is applied successively at each time level $n = 0,1,\ldots,N-1$.

The coefficient vector $\mathbf{C}^{n+1}$ obtained at each time level provides the numerical representation of the solution at that time.

The coefficient matrix depends on the current fractional order through the time-dependent coefficients θ_1^{n+1} and θ_2^{n+1}. Therefore, the matrix entries are updated at each time level, whereas its tridiagonal structure is preserved throughout the time-marching procedure.

The computational cost of solving the tridiagonal system at each time level is linear in the number of spatial unknowns. Hence, the use of the Thomas algorithm provides an efficient solution strategy for the spatial algebraic system while retaining the nonlocal temporal memory required by the variable-order fractional derivative.

6.4 Implementation Procedure

After the initialization stage, the numerical solution is advanced from t_n to t_{n+1} through a sequential time-marching procedure. At each time level, the variable fractional order is evaluated, the corresponding VO–L1 coefficients are computed, the temporal memory contribution is evaluated, and the fully discrete tridiagonal algebraic system is assembled. The Dirichlet boundary conditions are then incorporated through the boundary-elimination procedure, after which the resulting linear system is solved using the Thomas algorithm. Finally, the numerical solution is reconstructed from the updated spline coefficients. This procedure is repeated until the final time level is reached. The complete implementation is summarized in Algorithm 1.

7 Stability and Convergence Analysis

In this section, the stability and convergence properties of the proposed fully discrete cubic trigonometric B-spline collocation scheme combined with the variable-order L1 (VO–L1) approximation are analyzed.

The analysis is based on a discrete error equation obtained by comparing the fully discrete numerical formulation with the corresponding discrete relation satisfied by the exact solution. This error equation provides the starting point for the stability and convergence analysis of the proposed method.

The stability analysis takes into account the structure of the fully discrete coefficient matrix together with the positivity and monotonicity properties of the variable-order fractional memory weights established in Section 4. Under suitable assumptions on the discrete operator and its inverse, a stability estimate for the numerical solution is then derived.

Finally, the stability estimate is combined with the spatial and temporal consistency estimates of the cubic trigonometric B-spline collocation and VO–L1 discretizations, respectively, to establish a global error estimate for the fully discrete numerical method.

7.1 Error Equation

To derive the stability and convergence estimates, we first formulate the discrete error equation associated with the fully discrete scheme. Since the algebraic system is written in terms of the spline coefficients, the error is defined at the coefficient level. Let $\widetilde{C}_i^n$, denote the spline coefficient associated with the exact solution at time level t_n, and let C_i^n denote the corresponding numerical spline coefficient. We define the coefficient error by $e_i^n = \widetilde{C}_i^n - C_i^n$, $i = 0,1,\ldots,M$. Accordingly, the physical coefficient error vector is $\mathbf{e}^n = \left[e_0^n, e_1^n, \ldots, e_M^n\right]^T$. The

Algorithm 1 Fully discrete cubic trigonometric B-spline VO–L1 collocation method

1: Generate the uniform spatial and temporal grids $\{x_i\}_{i=0}^{M}$, $\{t_n\}_{n=0}^{N}$.
2: Compute the cubic trigonometric B-spline constants $A_1,\ldots,A_6$.
3: Initialize the spline coefficients by solving the initialization system together with the boundary conditions and the corresponding boundary-elimination relations.
4: **for** $n=0,1,\ldots,N-1$ **do**
5: Evaluate the variable fractional order $\lambda_{n+1}=\lambda(t_{n+1})$.
6: Compute the scaling factor γ_{n+1} and the VO–L1 weights a_k^{n+1}.
7: Evaluate the temporal memory contribution $\mathscr{H}_i^{n+1}$, $i=1,2,\ldots,M-1$, and set $\mathscr{H}_i^{1}=0$ for the first time step.
8: Apply the prescribed Dirichlet boundary conditions and eliminate the auxiliary spline coefficients C_{-1}^{n+1} and C_{M+1}^{n+1} using (8) and (9).
9: Determine the boundary spline coefficients C_0^{n+1} and C_M^{n+1} from the boundary collocation equations.
10: Assemble the interior tridiagonal coefficient matrix $\mathbf{K}_{\text{int}}^{n+1}$ for the unknown coefficients $\mathbf{C}_{\text{int}}^{n+1}=\left(C_1^{n+1},C_2^{n+1},\ldots,C_{M-1}^{n+1}\right)^{\mathsf{T}}$.
11: Assemble the interior right-hand-side vector $\mathbf{R}_{\text{int}}^{n+1}$, including the source term, previous-time-level contribution, temporal memory contribution, and boundary contributions.
12: Solve the interior tridiagonal linear system $\mathbf{K}_{\text{int}}^{n+1}\mathbf{C}_{\text{int}}^{n+1}=\mathbf{R}_{\text{int}}^{n+1}$ using the Thomas algorithm.
13: Recover the complete spline coefficient vector $\mathbf{C}^{n+1}=\left(C_0^{n+1},C_1^{n+1},\ldots,C_{M-1}^{n+1},C_M^{n+1}\right)^{\mathsf{T}}$, together with the auxiliary coefficients C_{-1}^{n+1} and C_{M+1}^{n+1} when required.
14: Recover the numerical solution at the collocation points from the updated spline coefficients using (5).
15: **end for**
16: Output the numerical solution.

exact solution, when substituted into the fully discrete collocation formulation, does not satisfy the discrete equations exactly because of the spatial and temporal discretization errors. We therefore denote the corresponding local consistency residual at the collocation point x_i and time level t_{n+1} by τ_i^{n+1}.

Subtracting the numerical fully discrete relation (21) from the corresponding discrete relation satisfied by the exact solution gives, for the interior collocation points $i=1,2,\ldots,M-1$,

$$\theta_1^{n+1}e_{i-1}^{n+1}+\theta_2^{n+1}e_i^{n+1}+\theta_1^{n+1}e_{i+1}^{n+1}=\gamma_{n+1}e_i^{n}+\gamma_{n+1}\sum_{k=1}^{n}a_k^{n+1}\left(e_i^{n-k+1}-e_i^{n-k}\right)+\tau_i^{n+1}. \tag{32}$$

Here, θ_1^{n+1} and θ_2^{n+1} are the time-level-dependent coefficient parameters defined in Section 6, while γ_{n+1} and a_k^{n+1} are the scaling factor and variable-order memory weights, respectively, introduced in Section 4. The quantity τ_i^{n+1} represents the local consistency residual resulting from the spatial and temporal discretizations.

For $n=0$, the history summation in (32) is empty and is therefore defined to be zero. Consequently, the error equation at the first time step reduces to

$$\theta_1^{1}e_{i-1}^{1}+\theta_2^{1}e_i^{1}+\theta_1^{1}e_{i+1}^{1}=\gamma_1 e_i^{0}+\tau_i^{1},\qquad i=1,2,\ldots,M-1. \tag{33}$$

For the interior equations, collecting the error components into the corresponding vector gives

$$\mathbf{K}_{\text{int}}^{n+1}\mathbf{e}_{\text{int}}^{n+1}=\gamma_{n+1}\mathbf{e}_{\text{int}}^{n}+\mathbf{H}_{e,\text{int}}^{n+1}+\tau_{\text{int}}^{n+1}, \tag{34}$$

where $\mathbf{e}_{\text{int}}^{n}=\left[e_1^n,e_2^n,\ldots,e_{M-1}^n\right]^T$ and $\tau_{\text{int}}^{n+1}=\left[\tau_1^{n+1},\tau_2^{n+1},\ldots,\tau_{M-1}^{n+1}\right]^T$. The discrete memory contribution is defined componentwise by

$$\left(\mathbf{H}_{e,\text{int}}^{n+1}\right)_i=\gamma_{n+1}\sum_{k=1}^{n}a_k^{n+1}\left(e_i^{n-k+1}-e_i^{n-k}\right),\qquad i=1,2,\ldots,M-1. \tag{35}$$

Thus, the interior error system has the same tridiagonal structure as the interior algebraic system derived in Section 6. In particular, $\mathbf{K}_{\text{int}}^{n+1}$ is given by the tridiagonal matrix (27), with diagonal and off-diagonal entries determined by θ_2^{n+1} and θ_1^{n+1}, respectively.

The boundary equations are treated consistently with the boundary elimination procedure described in Section 6. After elimination of the auxiliary spline coefficients, they provide the first and last rows of the full algebraic system. Therefore, if the stability analysis is performed for the complete coefficient vector $\mathbf{e}^n = \left[e_0^n, e_1^n, \ldots, e_M^n\right]^T$, the two boundary error relations must be included together with the interior error equations.

Accordingly, the complete error system can be written abstractly as

$$\mathbf{K}^{n+1}\mathbf{e}^{n+1} = \gamma_{n+1}\mathbf{e}^n + \mathbf{H}_e^{n+1} + \tau^{n+1}, \tag{36}$$

where $\mathbf{K}^{n+1}$ is the complete coefficient matrix defined in (30), $\mathbf{H}_e^{n+1}$ denotes the corresponding discrete memory contribution, and τ^{n+1} is the full consistency-error vector.

The representation (36) provides the appropriate framework for the subsequent stability analysis, while (34) describes the corresponding interior error equations.

7.2 Stability and Convergence

The stability and convergence properties of the proposed fully discrete variable-order L1 (VO–L1) cubic trigonometric B-spline collocation scheme are established in this subsection.

The analysis is based on the discrete error equation derived in Section 7.1. The stability estimate is obtained by studying the evolution of the discrete error under the action of the fully discrete coefficient matrix and the variable-order memory terms. In particular, the properties of the VO–L1 memory weights are used to control the accumulated contribution of the previous time levels.

Once the stability estimate has been established, the convergence result follows by combining stability with the consistency estimates of the temporal VO–L1 approximation and the spatial cubic trigonometric B-spline collocation discretization. The resulting estimate provides the global error bound of the fully discrete numerical method.

Theorem 1 (Stability)**.** *Assume that the fully discrete coefficient matrix $\mathbf{K}^{n+1}$ is nonsingular for every time level $n = 0, 1, \ldots, N-1$ and that there exists a positive constant C_K, independent of the spatial mesh size h_x, the time step h_t, and the time level n, such that*

$$\left\| (\mathbf{K}^{n+1})^{-1} \right\|_\infty \leq C_K.$$

Assume further that the variable-order memory weights satisfy the properties stated in Section 4. Then the discrete error generated by the fully discrete scheme remains bounded in the maximum norm. More precisely, there exists a constant $C > 0$, independent of h_x and h_t, such that

$$\max_{0\leq n\leq N} \|\mathbf{e}^n\|_\infty \leq C \left(\|\mathbf{e}^0\|_\infty + \max_{1\leq m\leq N} \|\tau^m\|_\infty \right), \tag{37}$$

where τ^m denotes the consistency-error vector.

Proof. Starting from the discrete error equation (36), we write

$$\mathbf{K}^{n+1}\mathbf{e}^{n+1} = \gamma_{n+1}\mathbf{e}^n + \mathbf{H}_e^{n+1} + \tau^{n+1}. \tag{38}$$

Since $\mathbf{K}^{n+1}$ is nonsingular, multiplication by $(\mathbf{K}^{n+1})^{-1}$ gives

$$\mathbf{e}^{n+1} = (\mathbf{K}^{n+1})^{-1} \left(\gamma_{n+1}\mathbf{e}^n + \mathbf{H}_e^{n+1} + \tau^{n+1} \right). \tag{39}$$

Taking the infinity norm and using the uniform bound on the inverse coefficient matrix yields

$$\|\mathbf{e}^{n+1}\|_\infty \leq C_K \left(|\gamma_{n+1}| \|\mathbf{e}^n\|_\infty + \|\mathbf{H}_e^{n+1}\|_\infty + \|\tau^{n+1}\|_\infty \right). \tag{40}$$

The discrete memory term is then estimated using the properties of the variable-order L1 weights established in Section 4. In particular, the accumulated history contribution can be bounded in terms of the previously computed error levels. Consequently, there exists a constant $C_M > 0$, independent of h_x, h_t, and n, such that

$$\|\mathbf{H}_e^{n+1}\|_\infty \leq C_M \max_{0\leq m\leq n} \|\mathbf{e}^m\|_\infty. \tag{41}$$

Combining (40) and (41), together with the uniform bound on the time-dependent coefficients, gives a recursive estimate of the form

$$\|\mathbf{e}^{n+1}\|_\infty \le C\left(\max_{0\le m\le n}\|\mathbf{e}^m\|_\infty + \|\tau^{n+1}\|_\infty\right), \tag{42}$$

where $C>0$ is independent of the discretization parameters.

Applying the appropriate discrete Grönwall-type argument to (42) yields

$$\max_{0\le n\le N}\|\mathbf{e}^n\|_\infty \le C\left(\|\mathbf{e}^0\|_\infty + \max_{1\le m\le N}\|\tau^m\|_\infty\right), \tag{43}$$

where the constant C is independent of h_x and h_t. Therefore, the proposed fully discrete VO–L1 cubic trigonometric B-spline collocation scheme is stable in the maximum norm. □

Theorem 2 (Convergence)**.** *Assume that the exact solution satisfies $\Phi \in C^{4,2}\left(\overline{\Omega}\times[0,T_F]\right)$ and that the assumptions of Theorem 1 hold. Suppose, furthermore, that the local truncation-error vector satisfies*

$$\|\tau^{n+1}\|_\infty \le C_\tau\left(h_x^2 + h_t^{2-\lambda_{n+1}}\right), \qquad 0\le n\le N-1, \tag{44}$$

where $C_\tau>0$ is independent of h_x, h_t, and n. Assume also that the initialization procedure satisfies $\|\mathbf{e}^0\|_\infty \le C_0 h_x^2$, where $C_0>0$ is independent of h_x. For convenience, let $\lambda_m := \lambda(t_m)$, $m=0,1,\dots,N$, and define $\lambda_{\max} := \max_{0\le t\le T_F}\lambda(t)$. Then the proposed fully discrete VO–L1 cubic trigonometric B-spline collocation scheme satisfies the global error estimate

$$\max_{0\le n\le N}\|\mathbf{e}^n\|_\infty \le C\left(h_x^2 + h_t^{2-\lambda_{\max}}\right), \tag{45}$$

where $C>0$ is independent of h_x and h_t.

Proof. From the stability estimate (37), we have

$$\max_{0\le n\le N}\|\mathbf{e}^n\|_\infty \le C\left(\|\mathbf{e}^0\|_\infty + \max_{1\le m\le N}\|\tau^m\|_\infty\right).$$

By the assumed initialization estimate,

$$\|\mathbf{e}^0\|_\infty \le C_0 h_x^2 = \mathcal{O}(h_x^2).$$

On the other hand, from (44),

$$\max_{1\le m\le N}\|\tau^m\|_\infty \le C_\tau\left(h_x^2 + \max_{1\le m\le N} h_t^{2-\lambda_m}\right).$$

Since $\lambda_m \le \lambda_{\max}$, we have $2-\lambda_m \ge 2-\lambda_{\max}$. Therefore, for $0<h_t\le 1$,

$$h_t^{2-\lambda_m} \le h_t^{2-\lambda_{\max}}.$$

Consequently,

$$\max_{1\le m\le N}\|\tau^m\|_\infty = \mathcal{O}\left(h_x^2 + h_t^{2-\lambda_{\max}}\right).$$

Substituting the above estimates into the stability bound yields

$$\max_{0\le n\le N}\|\mathbf{e}^n\|_\infty = \mathcal{O}\left(h_x^2 + h_t^{2-\lambda_{\max}}\right).$$

Hence, under the stated stability and consistency assumptions, the proposed fully discrete VO–L1 cubic trigonometric B-spline collocation method has a spatial error of order $\mathcal{O}(h_x^2)$ and a temporal error of order $\mathcal{O}(h_t^{2-\lambda_{\max}})$. This completes the proof. □

8 Numerical Experiments

This section presents a series of numerical experiments to assess the accuracy and convergence behavior of the proposed cubic trigonometric B-spline collocation method combined with the VO–L1 approximation for the variable-order Caputo fractional derivative. The numerical results are used to evaluate the practical performance of the proposed method and to provide numerical evidence supporting the theoretical convergence estimate established in Section 7.

All computations are carried out in MATLAB. To assess the numerical accuracy and convergence behavior, manufactured exact solutions are prescribed, and the corresponding source terms, initial conditions, and boundary conditions are constructed consistently so that the prescribed solutions satisfy the governing problem exactly.

8.1 Test Problem

Consider the variable-order time-fractional diffusion problem introduced in Section 2 on the computational domain $(x,t) \in [0,1] \times [0,T_F]$. For the manufactured-solution test, the exact solution is chosen as

$$\Phi(x,t) = e^x t^2. \tag{46}$$

The corresponding source term is constructed by substituting (46) into the governing equation (1). Thus,

$$\mathscr{F}(x,t) = {}_0^C\mathscr{D}_t^{\lambda(t)} \Phi(x,t) - \rho\, \Phi_{xx}(x,t).$$

For the prescribed exact solution, the variable-order Caputo derivative is given by

$${}_0^C\mathscr{D}_t^{\lambda(t)} \Phi(x,t) = \frac{2e^x}{\Gamma(3-\lambda(t))} t^{2-\lambda(t)},$$

while the second spatial derivative satisfies

$$\Phi_{xx}(x,t) = e^x t^2.$$

Consequently, the source term takes the form

$$\mathscr{F}(x,t) = e^x \left[\frac{2t^{2-\lambda(t)}}{\Gamma(3-\lambda(t))} - \rho t^2 \right].$$

The variable fractional order is chosen as

$$\lambda(t) = \frac{e^{-t}}{300}, \qquad 0 \le t \le T_F.$$

The function $\lambda(t) = \frac{e^{-t}}{300}$ is chosen because it is smooth, positive, and monotonically decreasing, while remaining within the admissible interval $(0,1)$. Its small maximum value also leads to a temporal convergence order that is very close to second order. Since $\lambda(t)$ is monotonically decreasing on $[0,T_F]$, its maximum value is attained at $t=0$ and is therefore

$$\lambda_{\max} = \lambda(0) = \frac{1}{300}.$$

According to the convergence estimate established in Section 7, the temporal error is expected to behave as

$$\mathscr{O}\left(h_t^{2-\lambda_{\max}}\right) = \mathscr{O}\left(h_t^{2-\frac{1}{300}}\right),$$

where

$$2-\lambda_{\max} = 2 - \frac{1}{300} \approx 1.9967,$$

which is very close to second-order convergence in time.

The initial and boundary data are obtained directly from the prescribed exact solution so that the manufactured solution satisfies the complete problem exactly. The numerical solution is then compared with (46) to compute the numerical errors and assess the observed spatial and temporal convergence rates.

8.2 Error Norms

The numerical accuracy of the proposed method is assessed using the discrete maximum-norm error and the root mean square error (RMSE). At each time level t_n, the maximum-norm error is defined by

$$E_\infty^n = \max_{0\le i\le M} \left|\Phi(x_i,t_n) - U_i^n\right|,$$

where U_i^n denotes the numerical approximation to $\Phi(x_i,t_n)$. The global maximum-norm error over the entire space–time grid is then given by

$$E_\infty = \max_{0\le n\le N} E_\infty^n.$$

To provide an additional measure of the overall error distribution over the space–time grid, the root mean square error is computed as

$$\mathrm{RMSE} = \left[\frac{1}{(M+1)(N+1)} \sum_{n=0}^{N} \sum_{i=0}^{M} |\Phi(x_i,t_n) - U_i^n|^2 \right]^{1/2}.$$

These error measures are used throughout the numerical experiments to quantify the accuracy of the proposed method and to assess its observed spatial and temporal convergence behavior in relation to the theoretical estimate established in Section 7.

8.3 Simultaneous Space-Time Refinement

To assess the overall convergence behavior of the proposed method, the spatial and temporal discretizations are refined simultaneously by choosing the same number of spatial and temporal subintervals, i.e., $M = N$. Since the computational domain is $[0,1] \times [0,T_F]$, the corresponding mesh sizes are $h_x = 1/M$ and $h_t = T_F/N = T_F/M$. Thus, both discretization parameters decrease at the same asymptotic rate as the mesh is refined.

For the variable-order function adopted in the present numerical experiments,

$$\lambda(t) = \frac{e^{-t}}{300}, \qquad 0 \le t \le T_F,$$

the fractional order is monotonically decreasing, and hence its maximum value is attained at $t = 0$. Therefore, $\lambda_{\max} = \lambda(0) = 1/300$, and the theoretical temporal convergence order is $2 - \lambda_{\max} = 2 - \frac{1}{300} \approx 1.9967$.

Accordingly, under the simultaneous refinement strategy $M = N$, the spatial error behaves as $\mathcal{O}(M^{-2})$, whereas the temporal error behaves as $\mathcal{O}(M^{-(2-\lambda_{\max})})$. Hence, the dominant theoretical convergence order is $2 - \lambda_{\max} \approx 1.9967$, which is practically indistinguishable from second-order convergence.

The numerical results obtained under this refinement strategy are reported in Table 1.

Table 1. Simultaneous space–time refinement with $M = N$.

$M = N$	RMSE	Rate	E_∞	Rate
20	5.3402×10^{-5}	–	1.6204×10^{-4}	–
40	1.3250×10^{-5}	2.0111	4.0465×10^{-5}	2.0019
80	3.2985×10^{-6}	2.0060	1.0110×10^{-5}	2.0007
160	8.2251×10^{-7}	2.0036	2.5266×10^{-6}	2.0002

The results in Table 1 show a systematic reduction in both the RMSE and the maximum-norm error as the spatial and temporal meshes are refined simultaneously. The observed convergence rates remain very close to two, which is consistent with the theoretical order $2 - \lambda_{\max} \approx 1.9967$. The slight difference between the theoretical order and the observed rates is expected and may arise from the combined spatial and temporal error contributions, as well as pre-asymptotic effects. Overall, the numerical results are in good agreement with the convergence estimate established in Theorem 2.

8.4 Spatial Convergence Study

To investigate the spatial convergence behavior of the proposed method, the number of time steps is fixed at $N = 2000$. This fine temporal discretization is employed to sufficiently reduce the temporal discretization error, thereby allowing the spatial convergence behavior of the method to be examined more accurately.

The spatial mesh is then successively refined while keeping the temporal discretization fixed. The corresponding numerical results are reported in Table 2.

The results in Table 2 show a systematic reduction in both the RMSE and the maximum-norm error as the spatial mesh is refined. The observed convergence rates approach two for both error measures, confirming the expected second-order spatial accuracy of the proposed cubic trigonometric B-spline collocation method.

Since a sufficiently fine temporal discretization is employed with $N = 2000$, the temporal error is expected to remain small relative to the spatial discretization error. Consequently, the observed convergence rates primarily reflect the spatial accuracy of the method, in agreement with the theoretical convergence estimate established in Theorem 2.

Table 2. Spatial convergence study with fixed $N = 2000$.

M	RMSE	Rate	E_∞	Rate
20	5.1874×10^{-5}	–	1.6262×10^{-4}	–
40	1.3117×10^{-5}	1.9835	4.0629×10^{-5}	2.0001
80	3.2988×10^{-6}	1.9912	1.0156×10^{-5}	2.0002
160	8.2718×10^{-7}	1.9961	2.5389×10^{-6}	2.0003

8.5 Temporal Convergence Study

To investigate the temporal convergence behavior of the proposed method, the spatial mesh is sufficiently refined by fixing $M = 2000$. The value $M = 2000$ was chosen to ensure that the spatial discretization error is negligible compared to the temporal discretization error. This fine spatial discretization is employed to sufficiently reduce the spatial discretization error, thereby allowing the temporal convergence behavior of the method to be examined more accurately.

The number of time steps is then successively increased while the spatial discretization is kept fixed. The corresponding numerical results are reported in Table 3.

Table 3. Temporal convergence study with fixed $M = 2000$.

N	RMSE	Rate	E_∞	Rate
20	5.7877×10^{-7}	–	9.6215×10^{-7}	–
40	1.6522×10^{-7}	1.8086	2.7844×10^{-7}	1.7889
80	4.4614×10^{-8}	1.8888	7.9070×10^{-8}	1.8162
160	1.0838×10^{-8}	2.0414	2.2033×10^{-8}	1.8435

The results in Table 3 demonstrate a systematic reduction in both the RMSE and the maximum-norm error as the temporal mesh is refined. The observed convergence rates generally increase with mesh refinement. In particular, the RMSE rate reaches approximately two on the finest temporal mesh, while the maximum-norm error also exhibits a clear improvement toward the theoretical temporal convergence order. Since, a sufficiently fine spatial discretization is employed with $M = 2000$, the spatial discretization error is expected to remain small relative to the temporal discretization error. Consequently, the observed convergence behavior primarily reflects the accuracy of the proposed VO–L1 temporal discretization.

The deviations from the theoretical asymptotic order observed on the coarser temporal meshes can be attributed to pre-asymptotic effects and to the nonlocal contribution of the variable-order fractional memory term. As the temporal mesh is refined, the observed rates exhibit a clear tendency toward the theoretical prediction $2 - \lambda_{\max} \approx 1.9967$, providing further numerical evidence in support of the convergence analysis of the proposed fully discrete scheme.

8.6 Pointwise Error Analysis

To further assess the accuracy of the proposed numerical method, a pointwise comparison between the exact and numerical solutions is performed at the final time level $t = T_F = 1$. The computations are carried out using the finest spatial grid considered in the numerical experiments, namely $M = 2000$, while the temporal discretization is chosen as $N = 160$.

Table 4 presents the exact solution, the corresponding numerical approximation, and the absolute error at several representative spatial locations. Since $\beta = 2$, the exact solution at the final time is $\Phi(x, T_F) = e^x$. The results in Table 4 show very close agreement between the numerical and exact solutions at the selected spatial locations. The absolute errors at the interior points are of the order of 10^{-9}, indicating that the proposed method provides a highly accurate approximation for the selected spatial and temporal discretizations.

The zero errors reported at the boundary points result from the direct imposition of the prescribed Dirichlet boundary conditions and should therefore not be interpreted as evidence of the interior numerical accuracy. Overall, the pointwise comparison provides additional numerical evidence that the proposed cubic trigonometric B-spline VO–L1 collocation method accurately reproduces the exact solution and is consistent with the stability and convergence results established in Section 7.

Table 4. Pointwise comparison between the exact and numerical solutions at $t = T_F = 1$ for $M = 2000$ and $N = 160$.

x	Exact	Numerical	Absolute Error
0.0	1.000000	1.000000	0.00×10^{0}
0.1	1.105171	1.105171	1.27×10^{-9}
0.2	1.221403	1.221403	2.33×10^{-9}
0.3	1.349859	1.349859	3.15×10^{-9}
0.4	1.491825	1.491825	3.71×10^{-9}
0.5	1.648721	1.648721	4.00×10^{-9}
0.6	1.822119	1.822119	3.99×10^{-9}
0.7	2.013753	2.013753	3.63×10^{-9}
0.8	2.225541	2.225541	2.88×10^{-9}
0.9	2.459603	2.459603	1.69×10^{-9}
1.0	2.718282	2.718282	0.00×10^{0}

8.7 Graphical Representation of Numerical Results

To complement the quantitative error analysis, graphical comparisons between the exact and numerical solutions, together with visualizations of the corresponding numerical errors, are presented in this subsection. All figures are generated using the finest spatial and temporal discretizations considered in this study, namely $M = 2000$ and $N = 160$.

Figure 1 compares the exact solution with the corresponding numerical approximation at several representative time levels. The two solutions exhibit close agreement at all selected time levels, providing a visual indication of the accuracy of the proposed method.

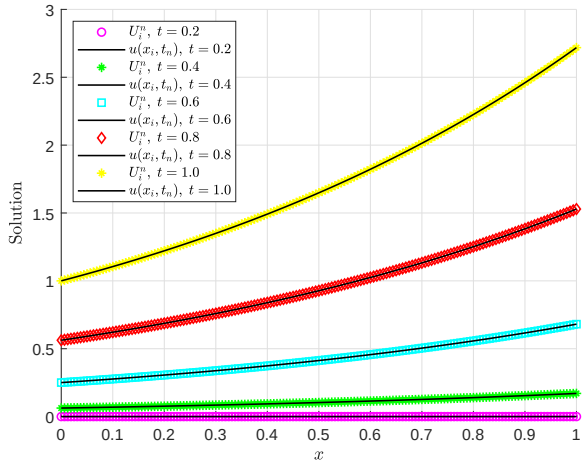


Figure 1. Comparison between the exact and numerical solutions at selected time levels for $M = 2000$ and $N = 160$.

Figure 2 illustrates the numerical solution over the entire space–time domain and shows the evolution of the computed solution throughout the simulation interval.

The distribution of the absolute error $|\Phi(x,t) - U(x,t)|$ over the computational domain is presented in Fig. 3. The error remains small over the space–time domain, which is consistent with the quantitative error measures reported in Tables 1–3.

Figure 4 shows the spatial distribution of the absolute error at the final simulation time $t = T_F$. The error remains small throughout the computational interval, in agreement with the spatial convergence behavior reported in Table 2.

Finally, Fig. 5 illustrates the temporal evolution of the absolute error during the simulation. The error remains small over the computational interval, consistent with the temporal convergence behavior reported in Table 3.

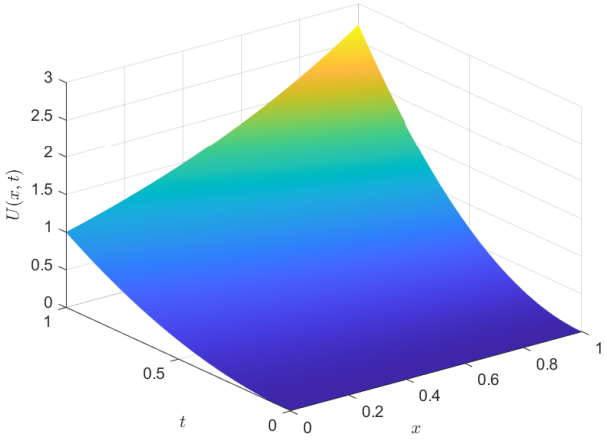


Figure 2. Numerical solution over the space–time domain for $M = 2000$ and $N = 160$.

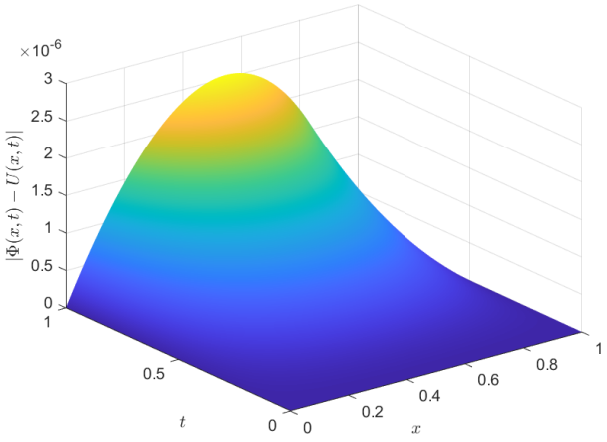


Figure 3. Absolute error surface over the space–time domain for $M = 2000$ and $N = 160$.

8.8 Discussion of Results

The numerical experiments presented in this section provide numerical evidence supporting the theoretical convergence properties of the proposed fully discrete cubic trigonometric B-spline VO–L1 collocation scheme. The simultaneous space–time refinement study shows a systematic reduction in both the RMSE and the maximum-norm error as the spatial and temporal meshes are refined. The observed convergence rates remain close to two, which is consistent with the theoretical convergence estimate established in Section 7. The spatial convergence study, performed with a sufficiently fine temporal discretization, confirms the expected second-order spatial accuracy of the cubic trigonometric B-spline collocation scheme. Similarly, the temporal convergence study, carried out with a sufficiently fine spatial mesh, shows convergence behavior consistent with the theoretical temporal order of $2 - \lambda_{\max}$ associated with the VO–L1 approximation. For the selected variable-order function $\lambda(t) = e^{-t}/300$, one has $\lambda_{\max} = 1/300$, so that the theoretical temporal order is $2 - \lambda_{\max} = 2 - \frac{1}{300} \approx 1.9967$, which is practically second order. The pointwise comparison and the graphical results further demonstrate the close agreement between the numerical and exact solutions over the computational domain. The error distributions remain small for the considered spatial and temporal discretizations, in agreement with the quantitative error measures reported in the preceding subsections.

Overall, the numerical results are consistent with the theoretical stability and convergence analysis presented in Section 7. In particular, they confirm the expected second-order spatial behavior and the nearly second-order temporal convergence predicted for the selected

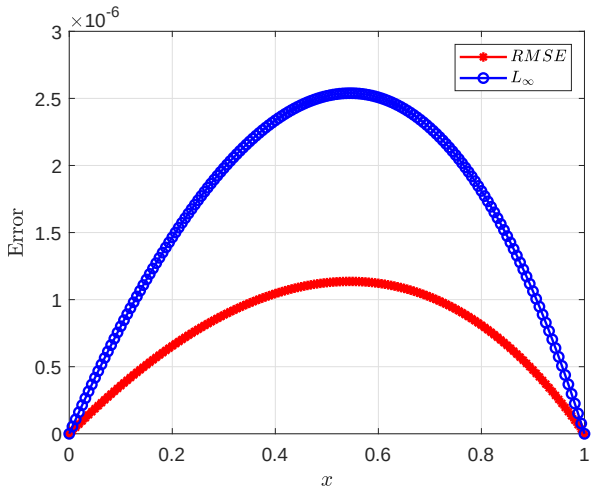


Figure 4. Spatial distribution of the numerical error at $t = T_F$ for $M = 2000$ and $N = 160$.

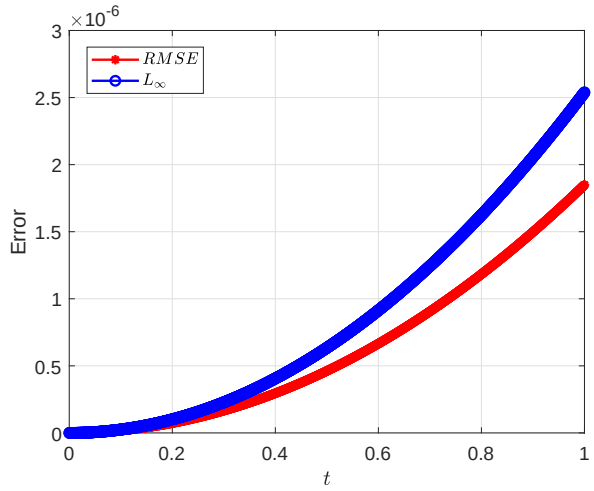


Figure 5. Temporal evolution of the numerical error for $M = 2000$ and $N = 160$.

variable-order fractional derivative. These results support the accuracy and numerical reliability of the proposed cubic trigonometric B-spline VO–L1 collocation method for the variable-order time-fractional diffusion problem considered in this work.

9 Conclusion

In this paper, a cubic trigonometric B-spline collocation method combined with the variable-order L1 (VO–L1) approximation has been proposed for the numerical solution of variable-order time-fractional diffusion equations. The proposed approach combines the spatial approximation capability of cubic trigonometric B-splines with the flexibility of the VO–L1 discretization for the variable-order Caputo fractional derivative.

A fully discrete formulation was constructed by coupling the spline-based spatial discretization with the VO–L1 temporal approximation. The resulting algebraic system has a tridiagonal structure, which allows an efficient solution by the Thomas algorithm. The Dirichlet boundary conditions are incorporated systematically into the resulting matrix formulation.

The theoretical analysis established the stability of the proposed fully discrete scheme under a uniform boundedness assumption on the inverse of the coefficient matrix. Furthermore, the convergence analysis showed that the global error is bounded by $\mathscr{O}\left(h_x^2 + h_t^{2-\lambda_{\max}}\right)$, where $\lambda_{\max} = \max_{0\le t\le T_F} \lambda(t)$. Thus, the method is second-order accurate in space, while its temporal convergence order is $2 - \lambda_{\max}$. For the

variable-order function considered in the numerical experiments, $\lambda_{\max} = 1/300$, giving a temporal order of approximately 1.9967, which is practically second order.

Several numerical experiments based on a manufactured exact solution were performed to assess the accuracy and convergence behavior of the proposed method. The numerical results showed a systematic reduction in both the RMSE and the maximum-norm error under mesh refinement. The spatial convergence study confirmed the expected second-order spatial accuracy, while the temporal convergence study exhibited rates consistent with the predicted high-order temporal convergence. The pointwise comparisons and graphical results also demonstrated close agreement between the numerical and exact solutions over the computational domain.

Overall, the theoretical and numerical results demonstrate that the proposed cubic trigonometric B-spline VO–L1 collocation method provides an accurate and stable numerical framework for the class of variable-order time-fractional diffusion problems considered in this work. The tridiagonal structure of the resulting algebraic system also supports an efficient computational implementation.

While the proposed method performs well for smooth variable-order functions and one-dimensional problems, its application to problems with non-smooth or rapidly changing orders requires further investigation. Additionally, the method currently relies on the assumption that the coefficient matrix remains nonsingular and that its inverse remains uniformly bounded for all considered discretization parameters. This assumption may require further analysis for extreme mesh sizes or more general problem settings. Extending the method to two- and three-dimensional problems, as well as to nonlinear variable-order fractional equations, represents a natural and important direction for future work. The development of more efficient memory-reduction techniques for large-scale, long-time simulations is also worth exploring.

Future research will therefore focus on extending the proposed methodology to multidimensional problems, nonlinear variable-order fractional models, and more general classes of variable-order fractional partial differential equations arising in scientific and engineering applications. In addition, the development of efficient memory-handling strategies and improved computational techniques for large-scale and long-time simulations will be considered.

Authors' Contributions

The conceptualization and methodology were developed by Javad Damirchi and Saedeh Foadian. The software coding, validation, and formal analysis were performed by Marzieh Khalili, who also conducted the primary investigation and data curation. All authors contributed to the writing, review, and editing of the manuscript. All authors have read and approved the final version.

Data Availability

The manuscript has no associated data or the data will not be deposited.

Conflicts of Interest

The authors declare no conflicts of interest regarding the publication of this paper.

Ethical Considerations

This study used a publicly available secondary dataset and did not involve direct human participation. Therefore, ethical approval was not required.

Funding

This research received no specific grant from any funding agency in the public, commercial, or not-for-profit sectors.

References

[1] I. Podlubny, Fractional Differential Equations, Academic Press, San Diego, 1999.

[2] K. Diethelm, N. J. Ford, A. D. Freed, A predictor–corrector approach for the numerical solution of fractional differential equations, Nonlinear Dynamics, 29, 3–22, (2002).

[3] G. Gao, Z. Sun, H. Zhang, A new fractional numerical differentiation formula to approximate the Caputo fractional derivative and its applications, Journal of Computational Physics, 259, 33–50, (2014).

[4] Y. Lin, C. Xu, Finite difference/spectral approximations for the time-fractional diffusion equation, Journal of Computational Physics, 225(2), 1533–1552, (2007).

[5] H. Sun, A. Chang, Y. Zhang, W. Chen, A review on variable-order fractional differential equations: mathematical foundations, physical models, numerical methods and applications, Fractional Calculus and Applied Analysis, 22(1), 27–59, (2019).

[6] M. Yousuf, S. Sarwar, Highly efficient numerical algorithm for nonlinear space variable-order fractional reaction–diffusion models, Fractal and Fractional, 7(9), 688, (2023).

[7] R. T. Sibatov, P. E. L'vov, H. Sun, Variable-order fractional diffusion: physical interpretation and simulation within the multiple trapping model, Applied Mathematics and Computation, 482, 128960, (2024).

[8] J.-L. Zhang, Z.-W. Fang, H.-W. Sun, Exponential-sum-approximation technique for variable-order time-fractional diffusion equations, Journal of Applied Mathematics and Computing, 68(1), 323–347, (2022).

[9] Y. Chen, J. Zhang, C. Pan, Numerical approximation of a variable-order time fractional advection-reaction-diffusion model via shifted Gegenbauer polynomials, AIMS Mathematics, 7(8), 15612–15632, (2022).

[10] S. Nemati, P. M. Lima, D. F. M. Torres, Numerical solution of variable-order fractional differential equations using Bernoulli polynomials, Fractal and Fractional, 5(4), 219, (2021).

[11] M. Yaseen, M. Abbas, M. B. Riaz, A collocation method based on cubic trigonometric B-splines for the numerical simulation of the time-fractional diffusion equation, Advances in Difference Equations, 2021(1), 210, (2021).

[12] M. Yaseen, M. Abbas, An efficient cubic trigonometric B-spline collocation scheme for the time-fractional telegraph equation, Applied Mathematics – A Journal of Chinese Universities, 35(3), 359–378, (2020).

[13] A. Esen, O. Tasbozan, Y. Ucar, N. M. Yagmurlu, A B-spline collocation method for solving fractional diffusion and fractional diffusion-wave equations, Tbilisi Mathematical Journal, 8(2), 181–193, (2015).

[14] J. Damirchi, S. Shagholi, S. Foadian, Cubic-B-spline collocation method for numerical solutions of the nonlinear fractional order Klein–Gordon equation, TWMS Journal of Applied Engineering Mathematics, 15(3), 526–537, (2025).

[15] A. Yazdani Cherati, Z. Azimi, The cubic trigonometric B-spline collocation method for the time-fractional stochastic advection-diffusion equation, International Journal of Nonlinear Analysis and Applications, 14(8), 161–167, (2023).

[16] R. Jiwari, S. Pandit, M. Köksal, A class of numerical algorithms based on cubic trigonometric B-spline functions for numerical simulation of nonlinear parabolic problems, Computational and Applied Mathematics, 38, 1–22, (2019).

[17] G. Arora, V. Joshi, A computational approach using modified trigonometric cubic B-spline for numerical solution of Burgers equation in one and two dimensions, Alexandria Engineering Journal, 57(2), 1087–1098, (2018).

[18] M. Shafiq, A. Fatima, M. Abbas, M. Alosaimi, F. A. Abdullah, An effective extended cubic B-spline approach for solving time-fractional diffusion-wave equation with exponential kernel, Alexandria Engineering Journal, 117, 148–163, (2025).